Supplemental Materials

Molecular Biology of the Cell

Tasaki *et al*.

Table S1. Plasmids, antibodies, and chemicals used in this study

Plasmid	**Reference**	**Identifier**
pRRLsinPPT-mCherry-C-hIFT144-IRES-Zeo	(Ishida *et al.*, 2021)	N/A
pRRLsinPPT-EGFP-C-hIFT43-IRES-Zeo	(Hirano *et al.*, 2017)	N/A
pRRLsinPPT-EGFP-C-hIFT52-IRES-Zeo	This study	N/A
pRRLsinPPT-EGFP-C-hIFT88-IRES-Blast	(Kobayashi *et al.*, 2021)	N/A
pRRLsinPPT-EGFP-C-hIFT88(1–805)-IRES-Blast	(Kobayashi *et al.*, 2021)	N/A
pRRLsinPPT-EGFP-C-hIFT144-IRES-Zeo	This study	N/A
pRRLsinPPT-EGFP-C-hIFT144(1–1102)-IRES-Zeo	(Ishida *et al.*, 2021)	N/A
pRRLsinPPT-EGFP-C-hDYNC2LI1-IRES-Blast	(Hamada *et al.*, 2018)	N/A
pRRLsinPPT-EGFP-N-B9D1-IRES-Blast	(Okazaki *et al.*, 2020)	N/A
pGEX6P1-GFP-Nanobody	(Katoh *et al.*, 2015)	Addgene 61838
pRSV-REV	(Thomas *et al.*, 2009)	Gift from Peter McPherson
pMD2.g	(Thomas *et al.*, 2009)	Gift from Peter McPherson
pMDLg/pRRE	(Thomas *et al.*, 2009)	Gift from Peter McPherson
Antibody	**Source or reference**	**Identifier**
Monoclonal mouse anti-Ac-α-tubulin (1:1,000 for IF)	Sigma-Aldrich	Clone 6-11B-1
Monoclonal mouse anti-CEP43 (1:10,000 for IF)	Abnova	Clone 2B1
Polyclonal rabbit anti-IFT38 (1:3,000 for IF; 1:5,000 for IB; 1:500 for U-ExM)	(Botilde *et al.*, 2013)	Gift from Hiroshi Hamada and Takanobu A. Katoh
Polyclonal rabbit anti-IFT88 (1:500 for IF)	Proteintech	13967-1-AP
Polyclonal rabbit anti-IFT140 (1:500 for IF and U-ExM; 1:1,000 for IB)	Proteintech	17460-1-AP
Monoclonal mouse anti-RFP (1:1,000 for IF)	MBL Life Science	Clone 3G5
Polyclonal chicken anti-GFP (1:1,000 for IF; 1:500 for U-ExM)	Aves Labs	GFP-1010
Monoclonal mouse anti-GFP (1:10,000 for IB)	Proteintech	66002-1-Ig
Polyclonal rabbit anti-IFT70 (1:1,000 for IB)	Proteintech	25352-1-AP
Polyclonal rabbit anti-IFT81 (1:1,000 for IB)	Proteintech	11744-1-AP
Polyclonal rabbit anti-IFT139 (1:1,000 for IB)	Human Protein Atlas	HPA035495
Monoclonal mouse anti-GAPDH (1:10,000 for IB)	Ambion	Clone 6c5
AlexaFluor-conjugated secondary (1:1,000 for IF and U-ExM)	Molecular Probes	A11034, A11039, A21137, A21147, A21242, A21429
Peroxidase-conjugated secondary (1:5,000 for IB)	Jackson ImmunoResearch	115-035-166, 111-035-144

Chemical	Source	Identifier
Polyethylenimine Max	Polysciences	24765-1
Blasticidin S	InvivoGen	ant-bl
Zeocin	InvivoGen	ant-zn
HEPES (4-(2-hydroxyethyl)-1-piperazineethanesulfonic acid)	Nacalai Tesque	17546-05
Potassium chloride	Nacalai Tesque	285-14
Sodium chloride	Nacalai Tesque	31320-05
Magnesium chloride hexahydrate	Nacalai Tesque	20909-55
Dithiothreitol	Nacalai Tesque	14112-52
Glycerol	Nacalai Tesque	17018-25
Polyethylene glycol Mono-*p*-isooctylphenyl ether	Nacalai Tesque	28828-93
Sodium acrylate	Sigma-Aldrich	408220
Acryl amide	Nacalai Tesque	00809-85
N,N′-methylenebisacrylamide	Nacalai Tesque	22402-02
N,N,N′,N′-tetramethylethylenediamine	Nacalai Tesque	33401-72
Ammonium persulfate	Nacalai Tesque	02627-34
Sodium dodecyl sulfate	Nacalai Tesque	31607-65
UltraPure Tris	Invitrogen	15504-020
Formaldehyde	Nacalai Tesque	16223-55
Tween 20	Nacalai Tesque	35624-15
SeaPlaque Agarose	Lonza	50100

IF, immunofluorescence; IB, immunoblotting: N/A, not applicable

Table S2. KO cell lines used in this study

Knocked out gene	Cell line	Reference
IFT52	#52-2-8	(Ishida *et al.*, 2022)
IFT54	#54-4-3	(Hiyamizu *et al.*, 2023)
IFT81	#81-1-4	(Tasaki *et al.*, 2023)
IFT88	#88-1-7	(Katoh *et al.*, 2017)
IFT144	#144-2-5	(Hirano *et al.*, 2017)
IFT139	#139-2-8	(Hirano *et al.*, 2017)
KIF3B	#3B-2-1	(Funabashi *et al.*, 2018)
DYNC2LI1	#LI1-3-2	(Qiu *et al.*, 2022)
WDR60	#W60-2-2	(Hamada *et al.*, 2018)

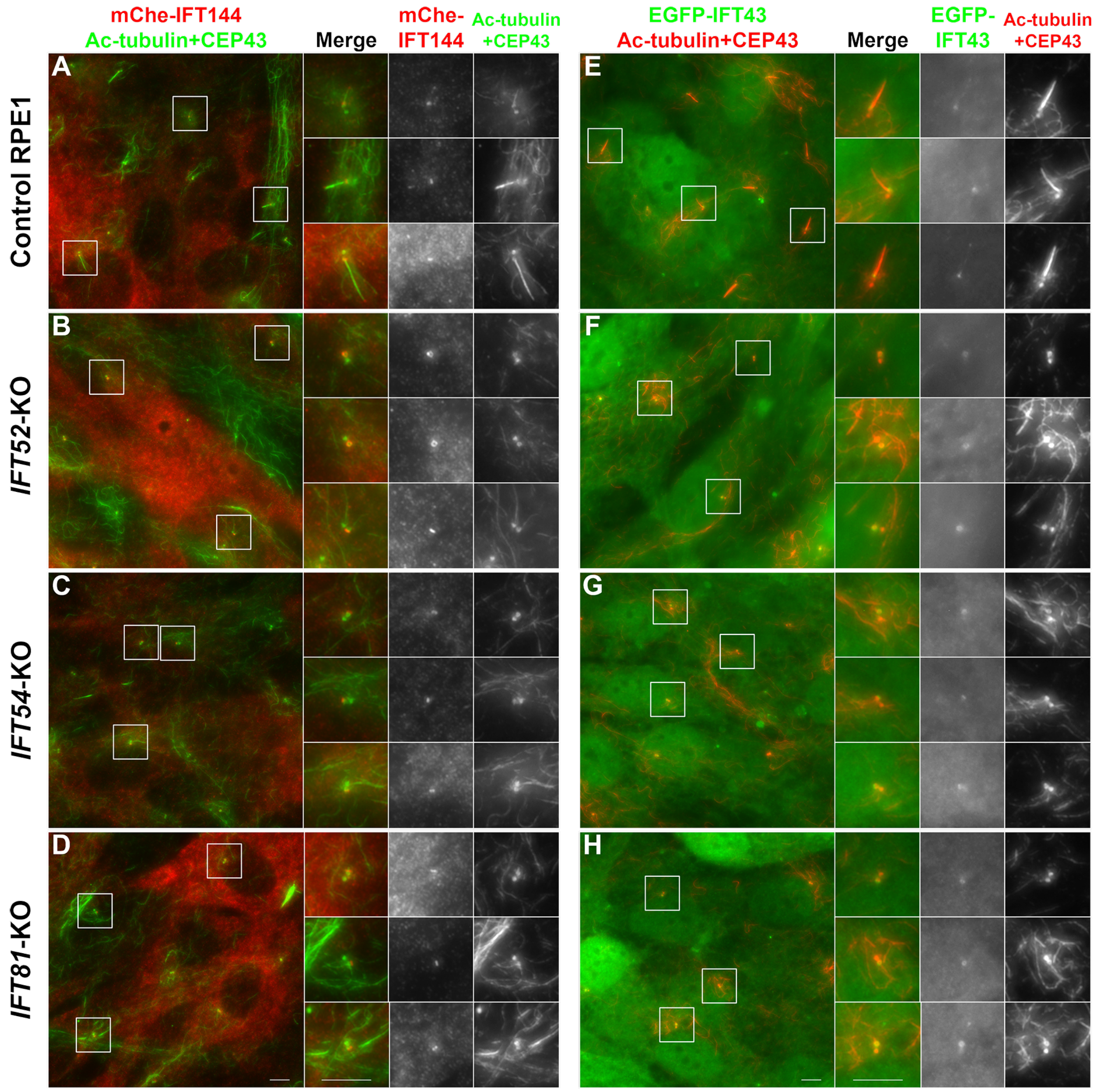

Fig. S1. IFT-A1 and IFT-A2 are recruited to the mother centriole in the absence of IFT-B subunits

Control RPE1 cells (A, E), IFT52-KO cells (B, F), IFT54-KO cels (C, G), and *IFT81*-KO cells (D, H) that stably express mCherry (mChe)-fused IFT144 (A–D) or EGFP-fused IFT43 (E–H) were cultured in serum-free medium for 24 h to induce ciliogenesis, and immunostained with antibodies against RFP (A–D) and Ac-tubulin+CEP43. Images shown on the right side are 2.5-times enlarged images of the boxed regions. Scale bars, 5 μm.

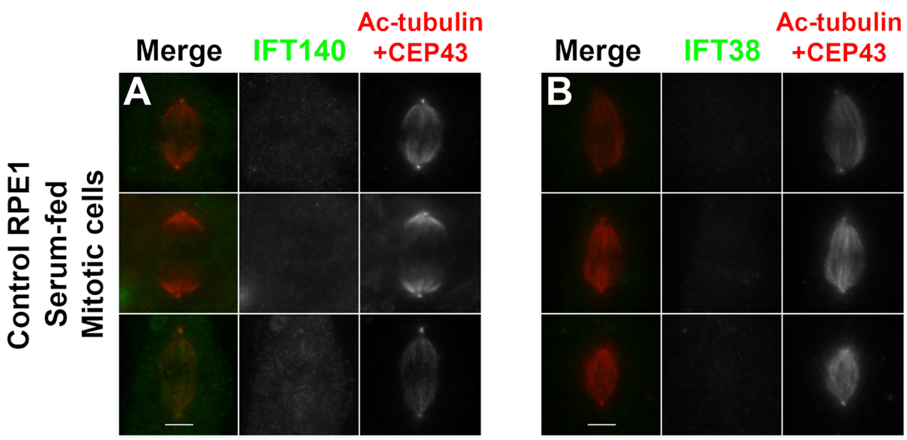

Fig. S2. IFT-A and IFT-B complexes were not present around the centrosomes in mitotic cells

(A, B) Serum-fed control RPE1 cells during mitosis were immunostained with antibodies against either IFT140 (A) or IFT38 (B), and Ac-tubulin+CEP43. Images of cells during mitosis are shown. Scale bars, 5 µm.

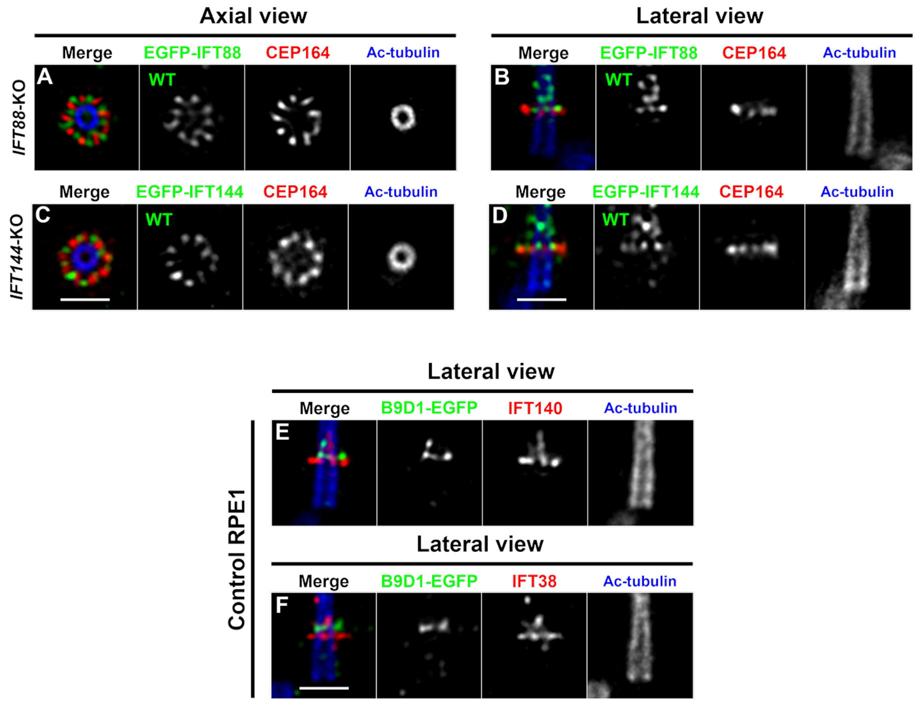

Fig. S3. IFT-A and IFT-B complexes are localized to DAPs and on the distal side of the TZ

(A–D) Axial (A, C) or lateral (B, D–F) views of the mother centriole in *IFT88*-KO cells stably expressing EGFP-IFT88(WT) (A, B), *IFT144*-KO cells stably expressing EGFP-IFT144(WT) (C, D), and control RPE1 cells stably expressing B9D1-EGFP (E, F). Serum-starved cells were expanded in superabsorbent hydrogels, and immunostained with antibodies against GFP and Ac-tubulin, and either CEP164 (A–D), IFT140 (E), or IFT38 (F), and Ac-tubulin. Scale bars, 2 µm

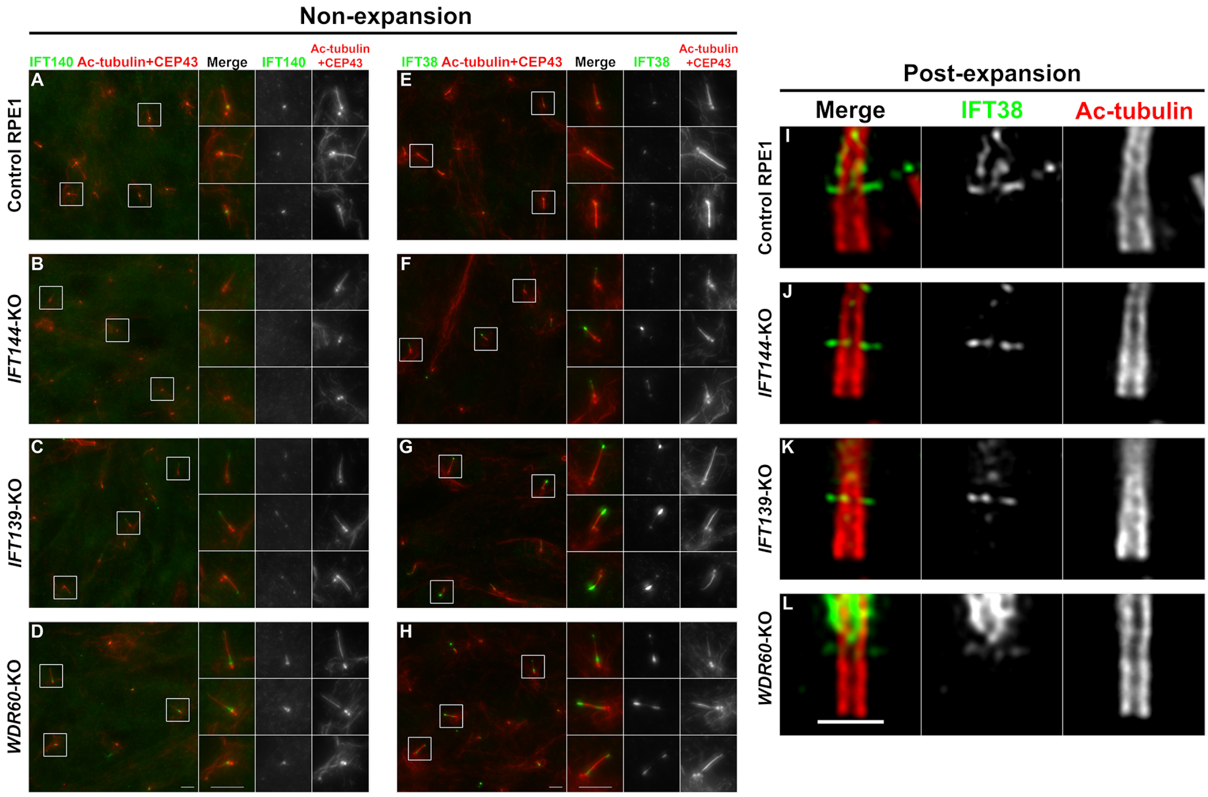

Fig. S4. Localization of retrograde IFT trains to the TZ revealed by U-ExM

(A–H) Nonexpanded control RPE1 cells (A, E), *IFT144*-KO cells (B, F), *IFT139*-KO cells (C, G), and *WDR60*-KO cells (D, H) were serum starved for 24 h, and immunostained with antibodies against either IFT140 (A–D) or IFT38 (E–H), and Ac-tubulin+CEP43. Images shown on the right side are 2.5-times enlarged images of the boxed regions. Scale bars, 5 µm. (I–L) Serum-starved control RPE1 cells (I), *IFT144*-KO cells (J), *IFT139*-KO cells (K), and *WDR60*-KO cells (L) were expanded in superabsorbent hydrogels, and immunostained with antibodies against IFT38 and Ac-tubulin. Scale bars, 2 µm

Supplemental References

Botilde, Y., Yoshiba, S., Shinohara, K., Hasegawa, T., Nishimura, H., Shiratori, H., and Hamada, H. (2013). Cluap1 localizes preferentially to the base and tip of cilia and is required for ciliogenesis in mouse embryo. Dev. Biol. *381*, 203-212.

Funabashi, T., Katoh, Y., Okazaki, M., Sugawa, M., and Nakayama, K. (2018). Interaction of heterotrimeric kinesin-II with IFT-B-connecting tetramer is crucial for ciliogenesis. J. Cell Biol. *217*, 2867-2876.

Hamada, Y., Tsurumi, Y., Nozaki, S., Katoh, Y., and Nakayama, K. (2018). Interaction of WDR60 intermediate chain with TCTEX1D2 light chain of the dynein-2 complex is crucial for ciliary protein trafficking. Mol. Biol. Cell *29*, 1628-1639.

Hirano, T., Katoh, Y., and Nakayama, K. (2017). Intraflagellar transport-A complex mediates ciliary entry as well as retrograde trafficking of ciliary G protein-coupled receptors. Mol. Biol. Cell *28*, 429-439.

Hiyamizu, S., Qiu, H., Tsurumi, Y., Hamada, Y., Katoh, Y., and Nakayama, K. (2023). Dynein-2–driven intraciliary retrograde trafficking indirectly requires multiple interactions of IFT54 in the IFT-B complex with the dynein-2 complex. Biol. Open *12*, bio059976.

Ishida, Y., Kobayashi, T., Chiba, S., Katoh, Y., and Nakayama, K. (2021). Molecular basis of ciliary defects caused by compound heterozygous *IFT144/WDR19* mutations found in cranioectodermal dysplasia. Hum. Mol. Genet. *30*, 213-225.

Ishida, Y., Tasaki, K., Katoh, Y., and Nakayama, K. (2022). Molecular basis underlying the ciliary defects caused by IFT52 variations found in skeletal ciliopathies. Mol. Biol. Cell *33*, ar83.

Katoh, Y., Michisaka, S., Nozaki, S., Funabashi, T., Hirano, T., Takei, R., and Nakayama, K. (2017). Practical method for targeted disruption of cilia-related genes by using CRISPR/Cas9-mediated homology-independent knock-in system. Mol. Biol. Cell *28*, 898-906.

Katoh, Y., Nozaki, S., Hartanto, D., Miyano, R., and Nakayama, K. (2015). Architectures of multisubunit complexes revealed by a visible immunoprecipitation assay using fluorescent fusion proteins. J. Cell Sci. *128*, 2351-2362.

Kobayashi, T., Ishida, Y., Hirano, T., Katoh, Y., and Nakayama, K. (2021). Cooperation of the IFT-A complex with the IFT-B complex is required for ciliary retrograde protein trafficking and GPCR import. Mol. Biol. Cell *32*, 45-56.

Okazaki, M., Kobayashi, T., Chiba, S., Takei, R., Liang, L., Nakayama, K., and Katoh, Y. (2020). Formation of the B9-domain protein complex MKS1–B9D2–B9D1 is essential as a diffusion barrier for ciliary membrane proteins. Mol. Biol. Cell *31*, 2259–2268.

Qiu, H., Tsurumi, Y., Katoh, Y., and Nakayama, K. (2022). Combinations of deletion and missense variations of the dynein-2 DYNC2LI1 subunit found in skeletal ciliopathies cause ciliary defects. Sci. Rep. *12*, 31.

Tasaki, K., Zhou, Z., Ishida, Y., Katoh, Y., and Nakayama, K. (2023). Compound heterozygous IFT81 variations in a skeletal ciliopathy patient cause Bardet-Biedl syndrome-like ciliary defects. Hum Mol Genet *32*, 2887-2900.

Thomas, S., Ritter, B., Verbich, D., Sanson, C., Bourbonnière, L., McKinney, R.A., and McPherson, P.S. (2009). Intersectin regulates dendritic spine development and somatodendritic endocytosis but not synaptic vesicle recycling in hippocampal neurons. J. Biol. Chem. *284*, 12410-12419.